Cellular/Molecular

RIM1α and RIM1β Are Synthesized from Distinct Promoters of the *RIM1* Gene to Mediate Differential But Overlapping Synaptic Functions

Pascal S. Kaeser,[1,3,4] Hyung-Bae Kwon,[6] Chiayu Q. Chiu,[6] Lunbin Deng,[1,3,4] Pablo E. Castillo,[6] and Thomas C. Südhof[1,2,3,4,5]

Departments of [1]Neuroscience and [2]Molecular Genetics, University of Texas Southwestern Medical Center, Dallas, Texas 75390-9111, [3]Institutes of Medicine and [4]Department of Molecular and Cellular Physiology, Stanford University, Palo Alto, California 94304-5543, [5]Howard Hughes Medical Institute and [6]Dominick P. Purpura Department of Neuroscience, Albert Einstein College of Medicine, Bronx, New York 10461

At a synapse, presynaptic terminals form a specialized area of the plasma membrane called the active zone that mediates neurotransmitter release. RIM1α is a multidomain protein that constitutes a central component of the active zone by binding to other active zone proteins such as Munc13 s, α-liprins, and ELKS, and to synaptic vesicle proteins such as Rab3 and synaptotagmin-1. In mice, knockout of RIM1α significantly impairs synaptic vesicle priming and presynaptic long-term plasticity, but is not lethal. We now find that the RIM1 gene encodes a second, previously unknown RIM1 isoform called RIM1β that is upregulated in RIM1α knock-out mice. RIM1β is identical to RIM1α except for the N terminus where RIM1β lacks the N-terminal Rab3-binding sequence of RIM1α. Using newly generated knock-out mice lacking both RIM1α and RIM1β, we demonstrate that different from the deletion of only RIM1α, deletion of both RIM1α and RIM1β severely impairs mouse survival. Electrophysiological analyses show that the RIM1αβ deletion abolishes long-term presynaptic plasticity, as does RIM1α deletion alone. In contrast, the impairment in synaptic strength and short-term synaptic plasticity that is caused by the RIM1α deletion is aggravated by the deletion of both RIM1α and RIM1β. Thus, our data indicate that the *RIM1* gene encodes two different isoforms that perform overlapping but distinct functions in neurotransmitter release.

Key words: **RIM; Rab3; Munc13; active zone; synaptic plasticity; neurotransmitter release**

Introduction

At a synapse, neurotransmitters are released by synaptic vesicle exocytosis at the presynaptic active zone (Katz and Miledi, 1967; Sudhof, 2004). Active zones are composed of a protein complex containing at least five proteins: RIMs, Munc13 s, ELKS, piccolo/bassoon, and α-liprins (Schoch and Gundelfinger, 2006). In addition, RIM-BPs, GIT, CASK, Velis, and Mints may also be present. Among these proteins, RIMs stand out because they are evolutionarily conserved scaffolding proteins that interact with many other active zone proteins, and perform central functions in synaptic vesicle exocytosis (Wang et al., 1997; Koushika et al., 2001; Schoch et al., 2002; Wang and Sudhof, 2003).

RIM1α constitutes the major RIM isoform that consists of an N-terminal short α-helix and zinc-finger domain, a central PDZ-domain, and two C-terminal C_2-domains (referred to as C_2A- and C_2B-domain) (for review, see Kaeser and Sudhof, 2005). The N-terminal α-helix of RIM1α binds to Rab3 (Wang et al., 1997), the zinc-finger binds to Munc13 s (Betz et al., 2001; Schoch et al., 2002; Dulubova et al., 2005), the PDZ-domain binds to ELKS (a.k.a., ERCs, CASTs, and Rab6IP2 s) (Nakata et al., 1999; Monier et al., 2002; Ohtsuka et al., 2002; Wang et al., 2002), and the C_2B-domain binds to α-liprins (Schoch et al., 2002). In addition, the RIM1α C_2-domains may interact with synaptotagmin-1, cAMP-GEFII, SNAP-25, and Ca^{2+}-channels, although these interactions remain controversial (Ozaki et al., 2000; Coppola et al., 2001; Hibino et al., 2002; Sun et al., 2003; Simsek-Duran et al., 2004; Dai et al., 2005; Kiyonaka et al., 2007). Finally, a PxxP sequence between the two C_2-domains of RIM1α binds to RIM-BPs (Wang et al., 2000), and the N-terminal region of RIM1α binds to 14-3-3 proteins (Sun et al., 2003; Simsek-Duran et al., 2004; Kaeser et al., 2008). Four *RIM* genes, *RIM1–RIM4*, are found in the mammalian genome. Only a single RIM1 isoform is known, RIM1α, but multiple RIM2 isoforms have been characterized: RIM2α that corresponds to RIM1α, RIM2β that lacks the N-terminal α-helix and zinc-finger of RIM2α, and RIM2γ that contains only the C_2B-domain. The *RIM3* and *RIM4* genes, finally, encode only γ-isoforms containing a single C_2B-domain (for review, see Kaeser and Sudhof, 2005).

RIM1α is essential for synaptic vesicle priming, short-term

Received July 11, 2008; revised Oct. 15, 2008; accepted Oct. 27, 2008.

This work was supported by National Institutes of Health grants from the National Institute of Neurological Disorders and Stroke (P01 NS053862) (T.C.S.) and the National Institute on Drug Abuse (DA17392) (P.E.C.), a Swiss National Science Foundation Postdoctoral Fellowship (P.S.K.), a National Alliance for Research on Schizophrenia (NARSAD) Young Investigator Award (P.S.K.), and a NARSAD Independent Investigator Award (P.E.C.). We thank E. Borowicz, J. Mitchell, I. Kornblum, and L. Fan for excellent technical assistance, Dr. R. H. Hammer for blastocyst injections of embryonic stem cells, and Dr. N. Brose for Munc13-1 antibodies.

Correspondence should be addressed to either of the following: Pascal S. Kaeser or Thomas C. Südhof, Institutes of Medicine and Department of Molecular and Cellular Physiology, Stanford University, 1050 Arastradero Road, Palo Alto, CA 94304-5543, E-mails: pkaeser@stanford.edu or tcs1@stanford.edu.

DOI:10.1523/JNEUROSCI.3235-08.2008

 0270-6474/08/2813435-13$15.00/0

synaptic plasticity, and presynaptic long-term plasticity (Castillo et al., 2002; Schoch et al., 2002; Calakos et al., 2004; Chevaleyre et al., 2007). At least the latter function depends on the RIM1α-interaction with Rab3 because deletion of Rab3A, the major Rab3 isoform, impairs presynaptic long-term plasticity similar to the RIM1α deletion, but does not replicate its other phenotypes (Castillo et al., 2002; Schoch et al., 2002). Furthermore, recent studies suggested RIM1α as a potential target for phosphorylation by SAD-kinase and ubiquitination, two processes that may be involved in regulating presynaptic neurotransmitter release (Inoue et al., 2006; Yao et al., 2007). Here, we demonstrate that the *RIM1* gene unexpectedly expresses a second, novel isoform called RIM1β that lacks the Rab3-binding α-helix. We generated mutant mice that lack both RIM1α and RIM1β, and demonstrate that these mice exhibit a much more severe phenotype than RIM1α-deficient mice, suggesting that RIM1α and RIM1β perform redundant roles in synaptic transmission to dictate active zone function.

Materials and Methods

Generation of conditional RIM1αβ knock-out mice. Conditional RIM1αβ knock-out (KO) mice were generated according to standard procedures (Rosahl et al., 1993; Ho et al., 2006) using homologous recombination in embryonic stem cells that targeted exon 6 of the RIM1 gene. The original targeting vector contained a serine 413 to alanine point mutation which was introduced to probe the effect of serine 413 phosphorylation of RIM1α (Kaeser et al., 2008). This point mutation was spontaneously repaired during homologous recombination in a subset of embryonic stem cells (Steeg et al., 1990; Maximov et al., 2008). By Southern blotting, PCR screening, and sequencing, we isolated these embryonic stem cells in which the *RIM1* gene was homologously recombined, but the serine 413 to alanine point mutation was repaired (see Results and supplemental materials, available at www.jneurosci.org). We used them for blastocyst injection to produce a conditional RIM1αβ KO mouse. The male chimeric offsprings were bred to C57BL/6 females, and tail DNA of the offsprings was used for genotyping by PCR and Southern blotting to indentify germ line transmission. The absence of the serine 413 to alanine point mutation in the mice was confirmed by *Bgl*I digest and DNA sequencing. Flp recombinase transgenic mice (Dymecki, 1996) and cre transgenic mice (O'Gorman et al., 1997) were used to remove the double-neomycin resistance cassette and to disrupt the *RIM1* gene, respectively. For a detailed description of the genomic clone, the targeting construct, and homologous recombination with a targeting construct that contained a serine 413 to alanine point mutation, see Kaeser et al. (2008), and supplemental Figure 3, available at www.jneurosci.org as supplemental material. The floxed, flp recombined allele was genotyped by PCR with oligonucleotide primers PK05163 (GACCGCTGTGCCAGGCGCACCTGC) and PK05164 (CCACAGTCTGCATTCCTACCCG). This reaction results in a 300 base pair (bp) wild-type band and a 400 bp floxed band. The KO allele was genotyped with PK04159 (GCAACGTTTGCTGCTGTAAGC 3) and PK04160 (CATTCTTGTCTCAACATTCAAGCC) to identify a 340 bp wild-type band and with PK04159 and PK05165 (CATCTTCACCTGCATCTCTGACC) to detect a 240 bp mutant band. All analyses were performed on littermate KO and wild-type offspring from heterozygous matings, and the genotypes were unknown to the experimenter.

5′RACE amplification and reverse transcriptase-PCR analysis. Total RNA was purified from the frontal cortex of 17-d-old RIM1α KO mice using a TRIzol Plus RNA Purification Kit (Invitrogen) according to the protocol delivered with the kit. 5′RACE amplification was performed with a 5′RACE amplification system form Invitrogen (Version 2.0) following the manufacturer's protocol. We used antisense oligonucleotides annealing to exon 6 of the RIM1 mRNA for reverse transcription (PK 06210, GGTTGCACCACAGACTTG) and two consecutive cycles of amplification with the oligonucleotide primers against the 5′ cap supplied with the kit and nested RIM1 oligonucleotide primers (PK 06211, GGGACACGTTTGCGCTC; PK 06212, CTCCCTTGCCATTCTGCTC). The product containing the new 5′ exon 1″ was sequenced and used for database analysis and reverse transcriptase-PCR (RT-PCR) oligonucleotide primer design. One-step RT-PCR was performed on RNA purified form the frontal cortex of 17-d-old RIM1α KO and RIM1αβ KO and control littermate mice with Superscript One-Step RT-PCR with Platinum *Taq* purchased from Invitrogen using oligonucleotide primers against RIM1α (PK 06206, CTTCACCGGGTAGCGAGCCAGG; PK 06216, ATCCGAAAGGTGAGAGCCAGAGC), RIM1β (PK 06217, CAAAGAACCACGCTCCAGATTTCG; PK 06218, GGGACATGTCACATGAGAGGAGAG) and control oligos for mouse neuroligin2/4* (MB30, GGAATTCCTACTGGACCAACTTCGCCAAGAC; MB31, GGAATTCGTCACGCTCAGCTCCGTCGAGTAG). The RT-PCR products were purified form an agarose gel and subjected to DNA sequencing.

Protein quantitations in S2 and P2 fractions of brain homogenates. Fractionation in a particulate (P2) and soluble (S2) fraction was essentially performed as previously described (Wang et al., 2002). In brief, brains were harvested from 3 pairs of RIM1αβ KO and wild-type littermate control mice at 8–9 weeks of age. Each brain was homogenized (in a detergent free buffer containing 25 mM HEPES, pH 7.2, 0.32 M sucrose, 5 mM EDTA, 1 mM PMSF, 1 μg/ml Leupeptin and Pepstatin, 2 μg/ml Aprotinin) using a motorized glass-Teflon homogenizer. After spinning for 10 min at 1500 × *g*, the postnuclear supernatant was centrifuged for 1 h at 162000 × *g* to separate P2 from S2. Protein contents were adjusted with a BCA protein assay kit (Pierce Biotechnology). Proteins (20 μg) were loaded per lane on standard SDS/PAGE gels for immunoblotting. Protein quantitations were done with ^{125}iodine-labeled secondary antibodies as previously described (Ho et al., 2006). We measured the levels of proteins in P2 and S2 with a Storm phosphoimager and normalized them to internal standards (valosin-containing protein, VCP, GDP dissociation inhibitor, GDI, or β-actin). Percentage of solubility was calculated by expressing the amount in S2 as a fraction of the total amount (P2+S2) without normalizing.

Electrophysiology in acute brain slices. Acute transverse hippocampal slices (400 μm thick) were prepared from 3- to 7-week-old mice. All recordings were performed at room temperature. The external solution for all experiments contained: 124 mM NaCl, 2.5 mM KCl, 26 mM $NaHCO_3$, 1 mM NaH_2PO_4, 2.5 mM $CaCl_2$, 1.3 mM $MgSO_4$ and 10 mM glucose. Extracellular field potentials were recorded either in CA1 stratum radiatum (to examine Schaffer collateral to CA1 pyramidal cell synapses), or in CA3 stratum lucidum (to examine mossy fiber to CA3 pyramidal cell synapses). Patch pipettes were filled with 1 M NaCl for extracellular recordings or with external solution for extracellular stimulation. Synaptic depression was examined using bursts of 25 stimuli at 14 Hz (90 s inter-burst intervals), and 5 responses were averaged for each experiment. Mossy fiber long-term potentiation (mf-LTP) was induced with 125 stimuli at 25 Hz in the presence of 50 μM D-APV. For the MK-801 experiments, EPSCs mediated by NMDARs were measured in whole cell voltage clamp from CA1 pyramidal neurons (+30 mV holding potential) in the presence of 10 μM NBQX and 100 μM Picrotoxin. The rate of MK-801 blockade of NMDAR-mediated EPSCs was assessed in ~2:1 Ca^{2+}:Mg^{2+} external solution at 0.1 Hz stimulation. After 10 min stable baseline synaptic responses, MK-801 (25 μM) was bath applied without stimulation for 8 min. Stimulation at 0.1 Hz was then resumed and the rate of blockade was determined. IPSCs in CA1 pyramidal cells (+10 mV holding potential) were evoked by stimulating GABAergic fibers in the middle third of stratum radiatum (0.05 or 0.1 Hz basal stimulation), and were monitored in the presence of 10 μM NBQX, 3 μM CGP 55845 and 25 μM D-APV. Recordings of miniature IPSCs (mIPSCs) were obtained under similar conditions, except that 1 μM TTX was also included in the bath to block action potentials. The intracellular solution contained the following: 131 mM Cs-Gluconate, 8 mM NaCl, 1 mM $CaCl_2$, 10 mM EGTA, 10 mM glucose, and 10 mM HEPES-CsOH, pH 7.2 (osmolarity 293 mmol/kg). Long-term depression at hippocampal inhibitory synapses (I-LTD) was elicited by theta-burst stimulation consisting of a series of 10 bursts repeated 4 times. Each burst was comprised of five 100 Hz stimuli and the inter-burst interval was 200 ms. Extracellular and whole-cell patch-clamp recordings were performed using a Multiclamp 700B amplifier (Axon Instruments). Stimulation and acquisition were

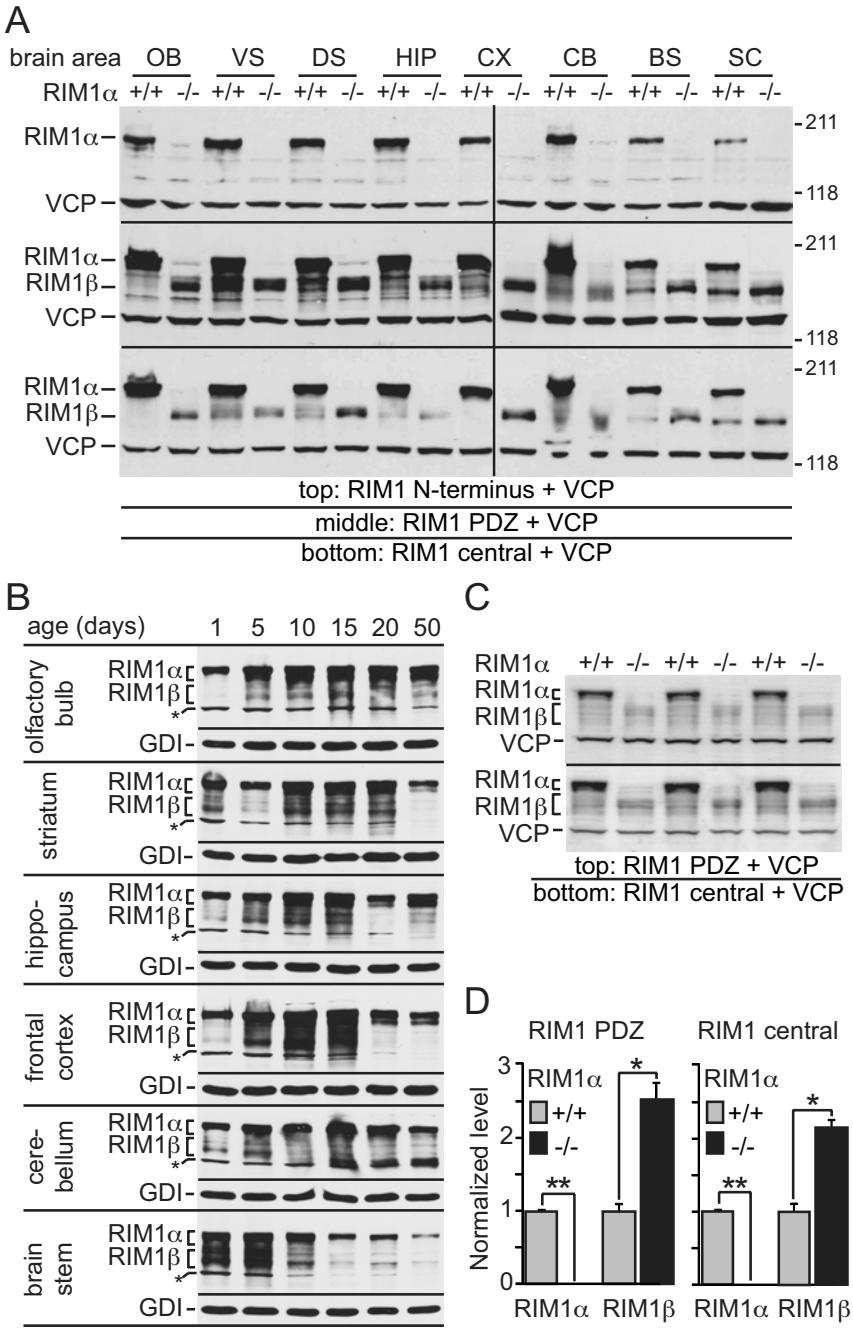

Figure 1. RIM1β is a new RIM1 isoform that is expressed throughout the brain. ***A***, Distribution of RIM1α and RIM1β in brain area homogenates of wild-type and littermate RIM1α KO mice at postnatal day 17. RIM1α and β were detected with antibodies against (from top to bottom) the RIM1α N terminus (polyclonal), the RIM1 PDZ domain (monoclonal) and the RIM1 central region (containing the PDZ domain and flanking regions, polyclonal). VCP was used as a loading control, protein size in kilo Dalton (kD) is indicated on the right. The following brain areas were used: OB, olfactory bulb; VS, ventral striatum; DS, dorsal striatum; HIP, hippocampus; CX, frontal cortex; CB, cerebellum; BS, brainstem; SC, spinal cord. ***B***, Regional and developmental expression profile of RIM1α and RIM1β in wild-type mice at postnatal days 1, 5, 10, 15, 20 and 50. RIM1α and β expression were assessed with the polyclonal antiserum against the RIM1 central region, and GDI was used as a loading control. *Cross-reactive band of unknown origin. ***C***, Quantitative immunoblotting with ^{125}iodine coupled secondary antibodies in 3 17-d-old RIM1α wild-type and KO littermate pairs with the monoclonal RIM1 PDZ domain antibody (top) and the polyclonal antiserum against the central domain (bottom). VCP antiserum was used as a loading control. ***D***, Quantitative analysis of RIM1α and RIM1β expression based on the Western blots shown in ***C***. RIM1α and β were normalized to the level of VCP. *$p < 0.05$, **$p < 0.005$.

controlled by custom written software in Igor Pro 4.09A (Wavemetrics). The paired-pulse ratio is defined as the ratio of the amplitude of the second synaptic response to the amplitude of the first synaptic response. The magnitude of mfLTP and I-LTD is calculated as the percentage change between baseline (averaged for 10 min before induction) and postinduction responses (50–60 min postinduction for mf-LTP; 20–30 min for I-LTD).

Electrophysiology in dissociated neuronal cultures. Hippocampi were isolated from new born mice (at postnatal day 1) and were digested using 0.5% trypsin-EDTA for 10 min at 37°C, and then separated by trituration. The neurons were plated in high density (~5000 cells/cm^2) onto coverslips pretreated with 2% matrigel (Collaborative Biomedical). For RIM1αβ conditional KO cultures, neurons from several mice were pooled and lentiviral infections were performed at 3–4 d *in vitro* (DIV) using a lentivirus encoding either a cre-EGFP fusion protein or a recombination deficient deletion mutant control. For the constitutive RIM1α KO cultures, mice were cultured individually, genotyped, and KO neurons and heterozygote control neurons were chosen for analysis. Whole-cell recordings were performed at DIV 13–16 using a multiclamp 700B amplifier (Axon Instruments) and an IPSC was elicited by a single or a paired electrical stimulation in the presence of 10 μM CNQX and 50 μM D-APV. The recording chamber was continuously perfused with bath solution (containing 150 mM NaCl, 4 mM KCl, 2 mM $CaCl_2$, 2 mM $MgCl_2$, 10 mM HEPES-NaOH, pH 7.3, and 10 mM glucose). Patch pipettes were pulled from borosilicate glass and back filled with 145 mM CsCl, 5 mM NaCl, 10 mM HEPES-CsOH, pH 7.3, 10 mM EGTA, 4 mM MgATP and 0.3 mM Na_2GTP. Data were collected with pClamp 9 software (Molecular Devices) sampled at 10 Hz and filtered at 1 Hz. Off-line measurements of IPSC amplitude and charge transfer were conducted using Clampfit software (Molecular Devices).

Miscellanous. PCR genotyping, Southern blotting, SDS/Page gels and immunoblotting were done according to standard methods (Ho et al., 2006). Mouse husbandry was performed according to institutional guidelines.

Statistical analysis. All data are shown as means ± SEMs unless otherwise stated. Statistical significance was determined by the Student's *t* test (two-tailed distribution, paired) for quantitative protein analysis, by χ test comparing the obtained ratio with an expected monogenic Mendelian ratio for mouse survival and recordings from cultured neurons. For electrophysiological recordings in acute hippocampal slices, statistical analysis was performed using Student's *t* test or one-way ANOVA at the $p < 0.05$ significance level in OriginPro 7.0 software (OriginLab).

Results

Discovery of RIM1β, a novel RIM1 isoform

To study the distribution of RIM1α in brain, we dissected multiple brain areas at postnatal day 17 of wild-type and RIM1α KO mice, and analyzed their constituent proteins by immunoblotting with multiple antibodies directed against RIM1α and control proteins (Fig. 1*A*). With an antibody against the RIM1α N terminus, we found that RIM1α was expressed throughout the brain, and was absent from RIM1α KO brains (Fig. 1*A*). RIM1α expression levels were

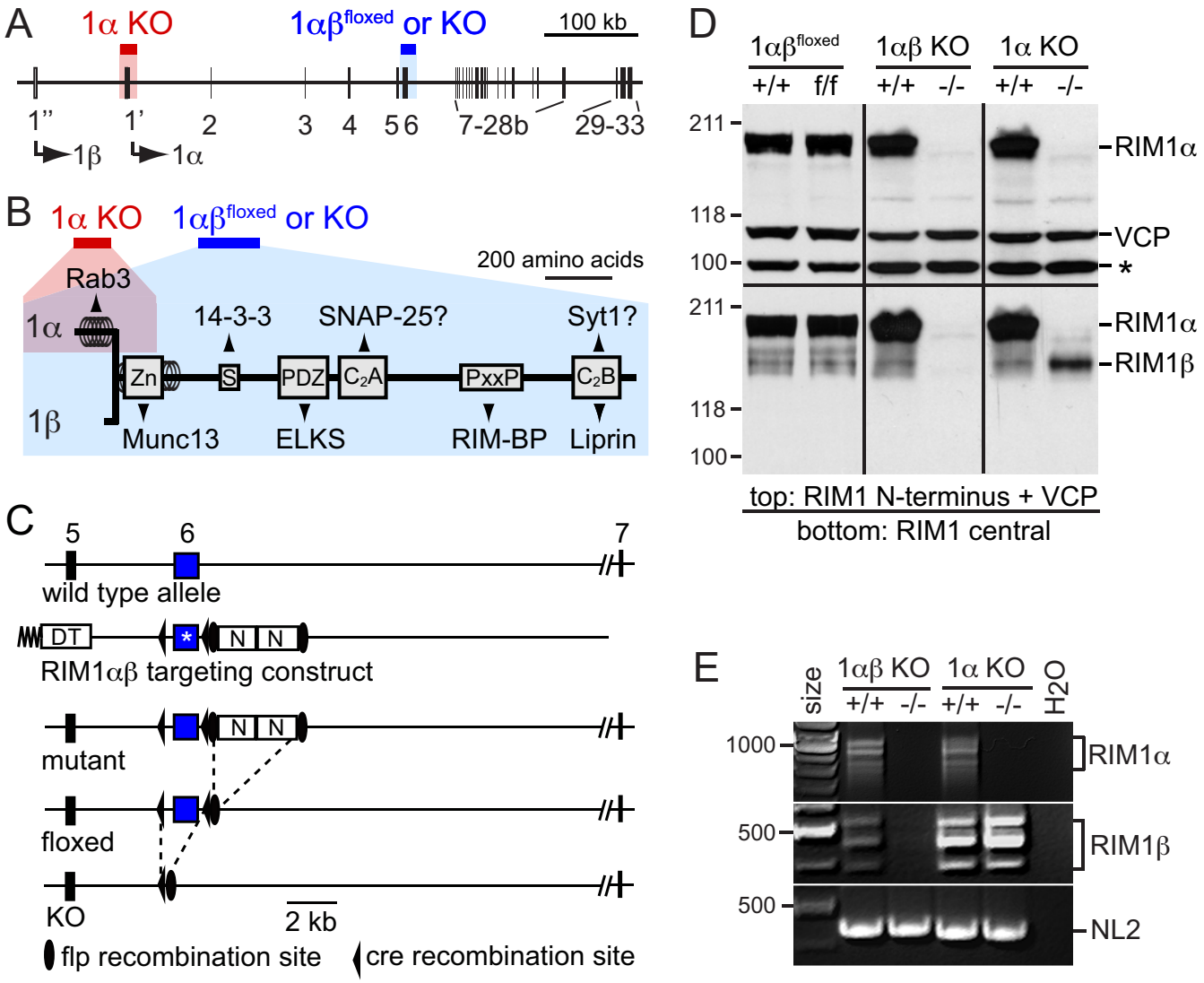

Figure 2. Generation and basic characterization of conditional RIM1αβ KO mice. ***A***, Map of the mouse *RIM1* gene (aka *Rims1*), alternative 5′ exons are marked with 1′ (for 1α) and 1″ (for 1β), respectively. The gene targeting experiments for RIM1α (red) and RIM1αβ (blue) are indicated. The gene is located in area 1A3 of chromosome 1. ***B***, Schematic representation of RIM1α and RIM1β, note that RIM1β lacks the helix α-1 at the N terminus (Zn, zinc finger domain; S, serine 413 residue; PxxP, proline rich region). Protein interactions with the active zone (bottom) or other presynaptic proteins (top) are indicated. The area and isoforms that were targeted in the RIM1α (red) and the RIM1αβ KO (blue) mice are indicated with bars and shaded backgrounds. ***C***, Targeting strategy for exon 6 of the *RIM1* gene, showing (from top to bottom) the wild-type allele, the targeting construct, the original mutant allele, the flp-recombined floxed allele and the cre recombined KO allele (DT, diphtheria toxin cassette; N, neomycin resistance cassette; * serine 413 to alanine point mutation that was repaired in the embryonic stem cells; 5–7, exons 5–7). ***D***, Immunoblotting of brain homogenates from RIM1αβ^{floxed}, RIM1αβ KO, RIM1α KO and wild-type littermate control mice (all at postnatal day 17) with an antibody against the RIM1 N terminus domain [top, *, crossreactivity with rabphilin (Schoch et al., 2002)] and the RIM1 central domain (bottom), protein size (kD) is indicated on the left. VCP was used as an internal control. ***E***, RT-PCR on mRNA purified from the frontal cortex of RIM1αβ KO mice, RIM1α KO mice and wild-type littermate control mice (all postnatal day 17), oligonucleotide primers for neuroligin 2/4* were used as a positive control, the 100 bp DNA ladder is indicated.

high in the forebrain (including olfactory bulb, ventral striatum, dorsal striatum, hippocampus and frontal cortex) and the cerebellum, and lower in the brainstem and the spinal cord. We confirmed these findings with a monoclonal antibody directed against the PDZ-domain of RIM1α, and a polyclonal antibody directed against the central region of RIM1α (the PDZ-domain and flanking areas). Unexpectedly, however, these two additional RIM1α antibodies detected a novel band in all brain regions at 160 kDa, and this band was specifically increased in RIM1α KO brains instead of being abolished (Fig. 1*A*).

We hypothesized that the new 160 kDa band may correspond to a new RIM1 isoform, and named it RIM1β in analogy to RIM2β produced by the *RIM2* gene (Wang et al., 2000). Immunoblotting showed that rat brain proteins also include a RIM1β variant (supplemental Fig. 1*A*, available at www.jneurosci.org as supplemental material), suggesting that RIM1β is evolutionarily conserved. The RIM1β band was expressed in a pattern similar to that of RIM1α, with a slightly higher relative expression in spinal cord and brainstem (Fig. 1*A*). To characterize the developmental and regional time course of RIM1β expression, we used brain region homogenates from wild-type mice at postnatal days 1, 5, 10, 15, 20 and 50 (Fig. 1*B*), and whole-brain homogenates from wild-type and RIM1α KO mice for a similar time course (supplemental Fig. 1*B*, available at www.jneurosci.org as supplemental material). We found that expression of RIM1β in forebrain and cerebellum is low at birth, increases during early postnatal development, and reaches a plateau that is around the detection limit in adulthood. In contrast, RIM1β has an accelerated expression

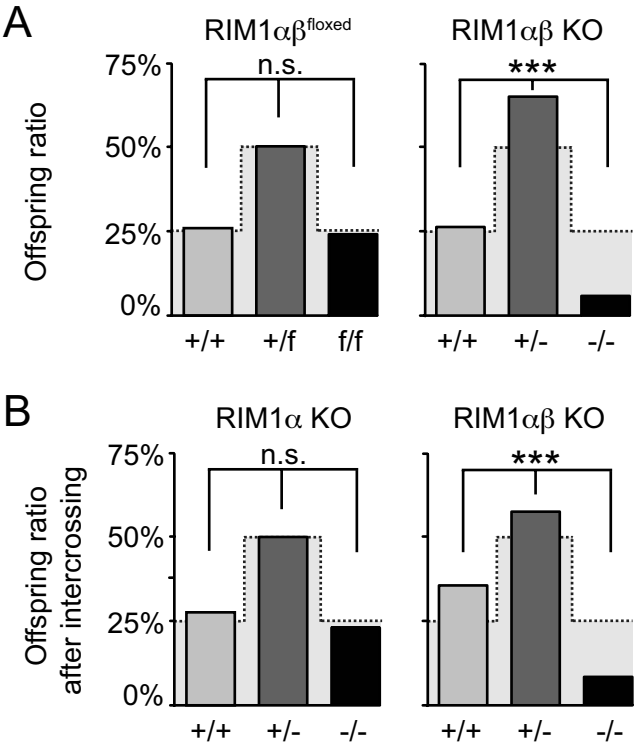

Figure 3. Survival is affected in RIM1αβ KO mice. ***A***, Survival rate in offsprings of heterozygous matings in the floxed and the KO line. *p* values were measured by χ test comparing the observed distribution with the expected Mendelian distribution (shaded background with dotted line; n.s., not significant, RIM1αβ KO, $p < 6.7 \times 10^{-18}$). ***B***, Survival rate in offsprings of heterozygous matings in the RIM1α KO and in the RIM1αβ KO mice after the genetic background of the two lines has been mixed for two generations (RIM1α KO not significant, RIM1αβ KO $p < 1.8 \times 10^{-4}$).

pattern in the brainstem where the levels are high early postnatally and decrease 10 d after birth. Although the relative expression level of RIM1β compared with RIM1α was pronounced in caudal brain areas (Fig. 1*A*,*B*), overall expression patterns are largely overlapping.

Because the immunoblotting experiments suggested that RIM1β is upregulated in RIM1α KO mice (Fig. 1*A*; supplemental Fig. 1, available at www.jneurosci.org as supplemental material), we quantified RIM1β expression in littermate wild-type and RIM1α KO mice with ^{125}iodine-labeled secondary antibodies. We found that RIM1β amounts to ~10–15% of RIM1α in wild-type mice, but was increased >2-fold in RIM1α KO mice (Fig. 1*C*,*D*; supplemental Table 1, available at www.jneurosci.org as supplemental material). As a result, RIM1β levels in RIM1α KO mice correspond to ~25% of wild-type RIM1.

Cloning of RIM1β

In the previously generated constitutive RIM1α KO mice, the first coding exon of RIM1α was replaced with a neomycin resistance cassette (Schoch et al., 2002). To search for an additional, shorter RIM1 isoform that does not include the first coding exon, and thus would not be abolished in the RIM1α KO mice, we purified mRNA from the frontal cortex of RIM1α KO mice and performed 5′ RACE amplification starting from exon 6. We identified a major 5′ RACE product that contained a new 5′ sequence, but lacked the sequences encoded by exons 1–3 of RIM1α, and thus does not contain the α-helical region of RIM1α that binds to Rab3A. Instead, the new 5′ sequence of RIM1β encodes a novel N-terminal 32 residue sequence without homology to known sequences (GenBank accession number FJ472653). Genome sequence searches revealed that this new 5′ sequence is encoded by a novel 5′ exon (referred to as exon 1″, compared with exon 1′ of RIM1α) 100 kb upstream of exon 1′of RIM1α on mouse chromosome 1 (Fig. 2*A*). A homologous sequence was detected in the 5′ end of the human *RIM1* gene, suggesting that RIM1β is a conserved RIM1 isoform that lacks the Rab3A-interacting α-helix, but is identical with RIM1α in all other protein domains C-terminal of this α-helix (Fig. 2*B*; supplemental Fig. 2, available at www.jneurosci.org as supplemental material). Importantly and in contrast to RIM2β, RIM1β therefore still contains the zinc-finger domain that binds to the C_2A domain of Munc13-1. Further analysis of the 5′ RACE products revealed that although exon 1′ of RIM1α that encodes the Rab3-binding α-helix was always absent from RIM1β mRNAs, the alternatively spliced exon 2 and exon 3 were variably present or absent in RIM1β mRNAs, suggesting that the first, RIM1α- and RIM1β-specific exons are transcribed from distinct promoters, but splice into the same differentially spliced exons downstream.

Generation of conditional RIM1αβ KO mice

To determine the functional significance of the transcription of two RIM1 isoforms, we generated conditional RIM1αβ KO mice. These were produced in parallel with a knockin mutant mouse line in which we introduced a serine 413 point mutation that abolishes protein kinase A phosphorylation of RIM1α (Kaeser et al., 2008). In brief, we generated a targeting vector in which we flanked exon 6 of the *RIM1* gene with cre/loxp recombination sites, and introduced a serine 413 to alanine point mutation (Fig. 2*C*). Embryonic stem cells were transfected with the *RIM1* targeting vector and we tested for homologous recombination by Southern blotting. Among clones containing a correctly recombined *RIM1* allele, one clone was isolated in which the serine 413 point mutation had been repaired, as confirmed by Southern blotting, PCR amplification and sequencing. This repair presumably occurred by a mismatch repair mechanism in embryonic stem cells (Steeg et al., 1990; Maximov et al., 2008), for a detailed description, see supplemental Figure 3, available at www.jneurosci.org as supplemental material. We produced chimeric mice that carry the floxed exon 6 according to standard procedures (Rosahl et al., 1993), and after germ line transmission, we removed the neomycin resistance gene with flp recombinase transgenic mice (Dymecki, 1996) to produce conditional RIM1αβ KO mice (referred to as RIM1αβ^{floxed} mice). The *RIM1* gene was disrupted in RIM1αβ^{floxed} mice by cre recombination in the male germ line (O'Gorman et al., 1997) to produce constitutive RIM1αβ KO mice (referred to as RIM1αβ KO mice).

We confirmed the correct conditional targeting of the *RIM1* gene by immunoblotting of whole-brain homogenates of adult RIM1αβ^{floxed} and RIM1αβ KO mice with multiple antibodies against RIM1, using constitutive RIM1α KO mice (Schoch et al., 2002) as a control (Fig. 2*D*). In RIM1αβ^{floxed} mice, RIM1α and RIM1β were expressed at levels similar to wild-type RIM1α and RIM1β. Both proteins were abolished in the RIM1αβ KO mice, whereas only RIM1α was abolished in RIM1α KO mice. We verified these results by RT-PCR on mRNA purified from the frontal cortex of RIM1α KO and RIM1αβ KO mice and wild-type littermates (Fig. 2*E*). In agreement with the immunoblotting results and the 5′RACE analysis, the RIM1α mRNA is undetectable in both mouse lines, and RIM1β is abolished in the RIM1αβ but not the RIM1α KO mice. Furthermore, sequencing of the RT-PCR products confirmed the existence of multiple combinations of the alternatively spliced exons 2 and 3 for both RIM1α and

RIM1β. Importantly, we could not detect an N-terminal protein fragment containing the RIM1 zinc finger domain in the RIM1αβ KO mice although we targeted the linker area between the zinc finger and the PDZ domain in these mice (supplemental Figs. 3, 4, available at www.jneurosci.org as supplemental material). Thus, our results confirm that RIM1β is a new, conserved RIM1 isoform expressed from the *RIM1* gene, and that cre recombination of the conditional RIM1αβ^{floxed} mice abolishes both RIM1 isoforms.

Deletion of RIM1α and RIM1β impairs mouse survival

When we analyzed the offspring of heterozygous matings of RIM1αβ^{floxed} mice, we observed that homozygous RIM1αβ^{floxed} mice survived at the expected Mendelian ratio (Fig. 3*A*). In contrast, we found that the offspring of heterozygous matings of RIM1αβ KO mice exhibited a skewed genotype ratio. The majority (~75%) of homozygous RIM1αβ KO mice die before postnatal day 7 (see supplemental Table 2, available at www.jneurosci.org as supplemental material, for the numerical values of mouse survival). This was unexpected, because the survival of the RIM1α KO mice is only slightly impaired (Schoch et al., 2002). To exclude a difference in genetic background as a confounding factor in the impaired survival of RIM1αβ KO mice and the near normal survival of RIM1α KO mice, we intercrossed RIM1α KO and RIM1αβ KO mice for two generations, and then separated the lines again to reanalyze survival for each individual line. This background mixing did not alter the normal survival of the RIM1α KO mice or the impaired survival of the RIM1αβ KO mice (Fig. 3*B*). When we compared these survival rates with the rates that were observed before background mixing, they were statistically unchanged (RIM1α before vs after mixing $p = 0.37$, RIM1αβ $p = 0.15$). We conclude that that the difference in survival between the original RIM1α KO mouse line and the new RIM1αβ KO mouse line is not due to genetic background effects, but is due to the combined loss of RIM1α and RIM1β.

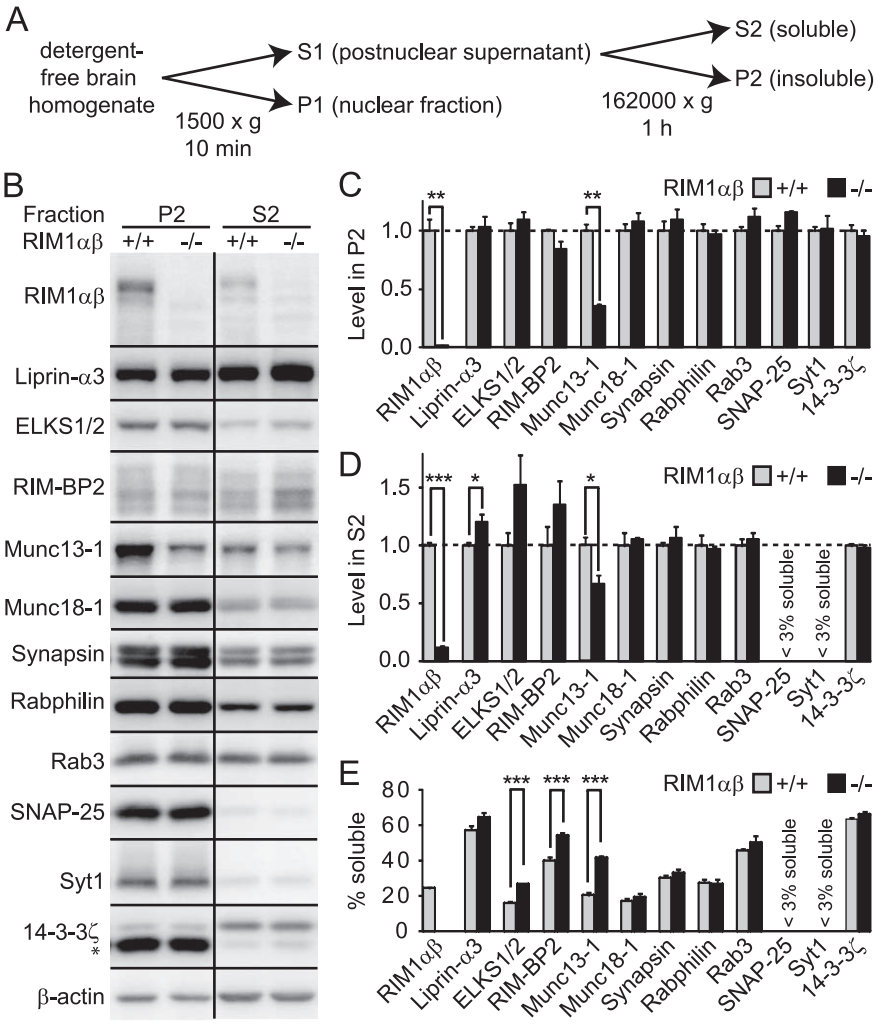

Figure 4. Protein quantitation in particulate (P2) and soluble (S2) fractions of RIM1αβ KO mice. ***A***, Schematic demonstration of the method used to generate the S2 and P2 fractions, arrows indicate centrifugation at the specified g-force and time. ***B***, Immunoblotting of P2 and S2 fractions with ^{125}iodine labeled secondary antibodies for multiple active zone and other proteins in brains from RIM1αβ KO mice and wild-type littermate controls ($n = 3$ for each fraction and genotype, all at 8–9 weeks of age, * marks SNAP-25, this antibody was added at the same time, but not used for quantitation). β-Actin is shown as a loading control. ***C***, ***D***, Quantitative analysis of protein contents in P2 (***C***) or S2 (***D***) normalized to VCP, GDI or β-actin. ***E***, Percentage of solubility expressed as S2*100/(P2+S2), solubility is not indicated when <3% of the total amount of protein were soluble (statistical significance in ***C–E***: *$p < 0.05$, **$p < 0.01$, ***$p < 0.005$). A more extensive list of proteins quantified can be found in supplemental Figure 5, available at www.jneurosci.org as supplemental material.

Increased solubility of RIM1 interacting active zone proteins in RIM1αβ KO animals

Presynaptic active zones are highly insoluble structures. RIMs are thought to be central components of these insoluble structures because they interact directly or indirectly with all other known components of presynaptic active zones. We thus tested whether the amounts and/or solubility of the RIM1-interaction partners and other neuronal proteins are changed in RIM1αβ KO mice. We prepared detergent-free brain homogenates from young adult RIM1αβ KO mice that are from the 20% surviving mice and from their wild-type littermate control mice, separated them into a particulate P2 fraction and a soluble S2 fraction by ultracentrifugation (Fig. 4*A*), and measured the levels of presynaptic and control proteins in wild-type and RIM1αβ KO mice by quantitative immunoblotting (Fig. 4*B–E*).

We found that Munc13-1 is reduced to 30% of wild-type levels in the particulate fraction of RIM1αβ KO mice, similar to the decrease in Munc13-1 in RIM1α KO mice (Schoch et al., 2002). The level of no other protein was affected (Fig. 4*B*, *C*; supplemental Table 3, available at www.jneurosci.org as supplemental material for the exact values of these quantitations). We then measured the same proteins in the soluble S2 fraction (Fig. 4*D*), and found that the levels of soluble liprin-α3 were slightly but significantly increased in RIM1αβ KO mice, while the levels of ELKS1/2 and of RIM-BP2 showed a nonsignificant trend toward an increase. Munc13-1 was decreased in S2, but to a lesser extent than in the particulate fraction. In calculating the % solubility for each protein that we quantified, we observed that ELKS1/2, RIM-BP2 and the remaining Munc13-1 were significantly more solu-

ble in RIM1αβ KO mice than in littermate control mice (Fig. 4*E*) (for the complete panel of proteins quantified, see supplemental Fig. 5 and supplemental Table 3, available at www.jneurosci.org as supplemental material). Thus, deletion of RIM1α and RIM1β causes a significant change in the association of several active zone proteins with the insoluble protein matrix of the active zone.

RIM1αβ KO mice display impaired excitatory synaptic transmission

To determine the participation of RIM1β in synaptic transmission, we measured synaptic responses in pyramidal neurons of area CA1 in the hippocampus in acute brain slices of RIM1αβ KO mice. This preparation has previously served to characterize the involvement of RIM1α in short-term plasticity (Schoch et al., 2002). Littermate wild-type and RIM1αβ KO mice were used, and the experimenter was unaware of the genotype of the mice analyzed. All values of the electrophysiological measurements in acute slices are listed in supplemental Table 4, available at www.jneurosci.org as supplemental material.

We first analyzed short-term plasticity at the excitatory Schaffer collateral to CA1 pyramidal cell synapse in acute brain slices of RIM1αβ KO mice. In measuring synaptic responses to paired stimuli at various interstimulus intervals (ISIs), we found that RIM1αβ KO mice showed increased facilitation, and this was more prominent at short ISIs compared with their wild-type littermates (Fig. 5*A*). We then measured synaptic responses to a short stimulus train (25 stimuli at 14 Hz), and again observed in RIM1αβ KO mice a massively increased facilitation that was maintained throughout the stimulus train. In contrast, wild-type synapses only showed a moderate facilitation during the first few stimuli that returned to baseline toward the end of the train (Fig. 5*B*). The RIM1αβ KO phenotype is similar to that of RIM1α KO mice, suggesting that deletion of RIM1α and RIM1β causes a reduction in the release probability P_r comparable with the deletion of RIM1α alone (Schoch et al., 2002). We then directly measured P_r in these synapses in the RIM1αβ KO mice (Fig. 5*C*). MK-801 irreversibly blocks NMDA receptors after activation by synaptic glutamate release. During repetitive stimulation, the rate of decrease of the NMDA receptor mediated synaptic response after application of MK-801 is directly proportional to P_r (Hessler et al., 1993; Rosenmund et al., 1993). In the RIM1αβ KO mice, the size of the EPSC responses during repetitive stimulation at 0.1 Hz declined slower compared with wild-type littermate controls. The rate of block was fitted by a second-order exponential decay, and we found that the time constant τ of the faster decay was ~2-fold increased after deletion of RIM1α and β (Fig. 5*C*), confirming a reduction of P_r similar to the one observed in the RIM1α KO animals (Schoch et al., 2002).

RIM1αβ KO mice display a prominent impairment in inhibitory synaptic transmission

We next analyzed inhibitory synaptic transmission in RIM1αβ KO mice. Because the role of RIM1α in inhibitory synapses is less well understood than its role in excitatory synapses (Schoch et al., 2002), we also analyzed RIM1α KO mice in these experiments, and directly compared RIM1α KO and RIM1αβ KO mice side-by-side for all parameters. The frequency of mIPSCs was reduced in both lines (Fig. 6*A*,*B*), but the effect was stronger in the RIM1αβ KO than in the RIM1α KO mice. The mIPSC amplitudes were unchanged in both lines. The decrease in mIPSC frequency suggests a presynaptic defect that is pronounced by the absence of RIM1β. The kinetics as expressed by rise time and time constant of decay of miniature release in these KO mice were

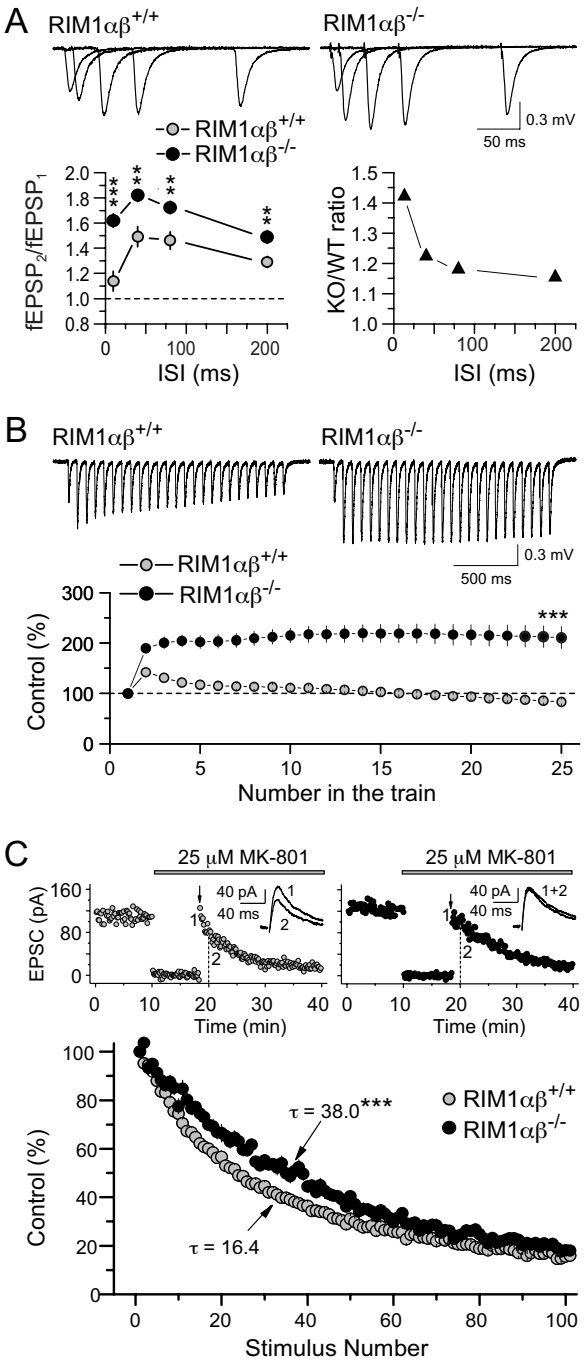

Figure 5. Short-term synaptic plasticity at excitatory Schaffer collateral to CA1 pyramidal cell synapses. ***A***, Paired-pulse facilitation ($fEPSP_2/fEPSP_1$) measured at 10, 40, 80, and 200 ms ISI in wild-type and RIM1αβ KO animals. Bottom graphs show summary data (left) and ratio of the paired-pulse facilitation values between KO to wild-type mice (right). Sample traces (superimposed after subtraction of the first response) are shown above. Statistical significance: $^{**}p < 0.005$, $^{***}p < 0.0005$. ***B***, Synaptic responses evoked by a burst of 25 stimuli at 14 Hz in wild-type and RIM1αβ KO mice (responses were normalized to the first fEPSP in the train). Representative responses are shown above. Statistical significance (sample values are given in supplemental Table 4, available at www.jneurosci.org as supplemental material): $^{***}p < 0.0001$. ***C***, Release probability in RIM1αβ KO mice and wild-type littermate controls as assessed by MK-801 block of NMDAR-EPSCs at 0.1 Hz stimulation. Representative single experiments are shown on top, afferent stimulation is stopped for 8 min during wash-in of MK-801, arrow marks the time when stimulation is resumed. Insets, NMDAR-EPSCs averaged from responses evoked by stimuli #1–3 and #11–13 at times indicated. For the summary time course of MK-801 block (bottom), the rate was fitted by second-order exponential decay, with the first time constant τ (in stimulus #) provided in the graph. Statistical significance for τ (RIM1αβ wild-type vs RIM1αβ KO): $^{***}p < 0.0001$.

unchanged in the absence of RIM1α and RIM1β, supporting that the effect of RIM1 deletion is presynaptic (supplemental Fig. 6, available at www.jneurosci.org as supplemental material). We next measured evoked neurotransmission (eIPSC amplitudes) in response to increasing stimulus intensities, and plotted the data as input-output curves (Fig. 6*C*,*D*). Similar to the mIPSC frequency, we found that deletion of RIM1α and RIM1β together had a stronger effect on evoked inhibitory synaptic transmission than deletion of RIM1α alone.

RIM1β contributes to short-term plasticity at inhibitory synapses

Inhibitory synapses usually express paired pulse depression, probably due to their high initial P_r. In a previous study (Schoch et al., 2002), inhibitory paired pulse depression was moderately increased in the RIM1α KO mice at short ISIs, but normal at longer ISIs at high initial P_r. When P_r was lowered by lowering the external calcium concentration, the RIM1α KO mice showed a reduction in facilitation, suggesting that P_r was increased in the absence of RIM1α (Schoch et al., 2002). This observation was puzzling, because it was contrary to the effect of RIM1α deletion in excitatory synapses. Therefore, we tested whether the additional deletion of RIM1β had an effect on responses to paired stimuli at these CA1 inhibitory synapses by directly comparing RIM1α and RIM1αβ KO mice (Fig. 7*A*,*B*). The RIM1α KO synapses showed paired pulse depression at all ISIs that was indistinguishable from wild-type littermates. In strong contrast, this depression was markedly decreased at all ISIs in the RIM1αβ KO mice, and this effect was much stronger at short ISIs as evidenced by the KO/wild-type ratio (Fig. 7*C*,*D*). This decreased depression in response to paired pulses together with the decreased mIPSC frequency is reminiscent of a reduction in P_r at inhibitory synapses in RIM1αβ KO mice.

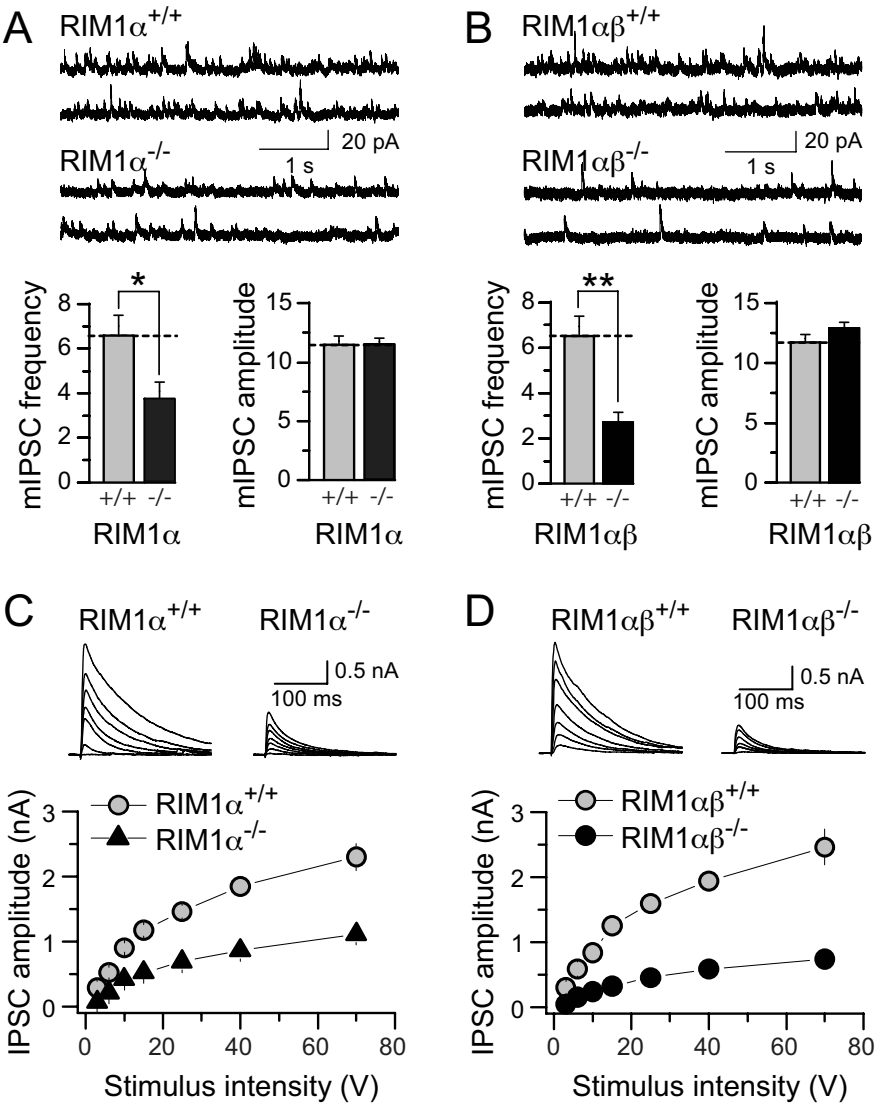

Figure 6. Miniature and evoked inhibitory synaptic transmission in the CA1 region of RIM1α KO and RIM1αβ KO mice. ***A***, ***B***, mIPSC frequencies and amplitudes monitored in CA1 pyramidal cells of RIM1α KO mice (***A***) and RIM1αβ KO mice (***B***) compared with wild-type littermate controls. Representative mIPSC traces are shown on top. Statistical significance: $*p < 0.05$, $**p < 0.005$. ***C***, ***D***, Evoked IPSC amplitudes plotted as a function of stimulation intensity. Representative traces from each stimulus intensity (3, 6, 10, 15, 25, 40, and 70 V) are shown, each trace is the average of 3–5 responses. Sample values for statistical significance: (***C***) 6 V: $p < 0.01$; 25 V: $p < 0.0001$; 70 V: $p < 0.00001$; (***D***) 6 V: $p < 0.005$; 25 V and 70 V: $p < 0.00001$.

RIM1αβ-deficient cultured neurons also exhibit impaired inhibitory synaptic transmission

The findings above suggest that the deletion of RIM1β has a specific effect on P_r of inhibitory synapses, that is absent in RIM1α KO mice. To confirm and extend our findings, we chose a second system to characterize inhibitory synaptic transmission which was previously described (Ho et al., 2006; Maximov et al., 2007). Cultured hippocampal neurons from homozygous RIM1αβ^{floxed} mice were infected with lentivirus expressing GFP-tagged cre-recombinase (RIM1αβ$^{f/f}$:cre) or a recombination deficient deletion mutant (RIM1αβ$^{f/f}$:control). At 13–16 d *in vitro*, we measured inhibitory synaptic currents in patch-clamp mode in response to single action potentials. Again, we are comparing these results with recordings from cultured neurons that were derived from either homozygous test or heterozygous control RIM1α KO mice (Fig. 8). We first measured single evoked IPSCs, and we found a strong reduction when either RIM1α alone or both RIM1α and RIM1β were absent (Fig. 8*A*,*B*). We then measured paired pulse responses and we found that RIM1α KO neurons showed a moderate decrease in paired pulse depression. The decrease was more pronounced when both RIM1 isoforms were deleted (Fig. 8*C*,*D*), as evidenced by the KO/control ratios (Fig. 8*E*,*F*). Detailed values of these *in vitro* experiments can be found in supplemental Table 5, available at www.jneurosci.org as supplemental material. It is important to note that the experiments for the RIM1α and the RIM1αβ deficient neurons were not done simultaneously, and that this is likely the cause of the observation that the paired pulse ratios in the control conditions vary between the two experiments. However, the data show that the deletion of RIM1αβ affects short-term plasticity in cultured neurons to a larger extent than deletion of RIM1α alone. The observation that

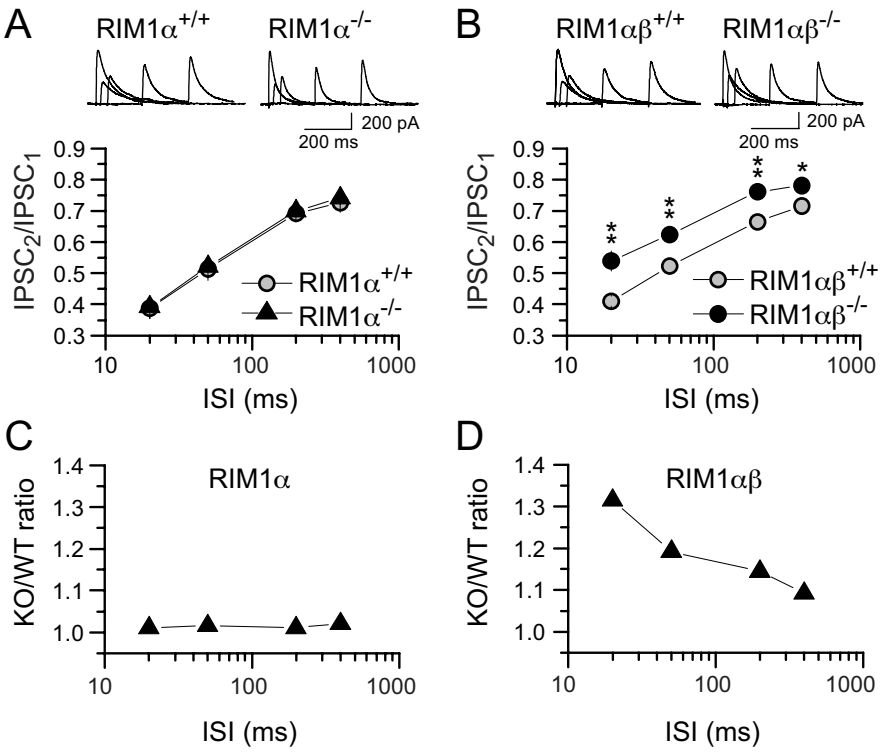

Figure 7. Short-term synaptic plasticity in inhibitory synapses in the CA1 region of RIM1α KO and RIM1αβ KO mice. ***A***, ***B***, Paired-pulse ratio ($IPSC_2/IPSC_1$) of evoked IPSCs measured at 20, 50, 200, and 400 ms ISI in RIM1α KO (***A***) and RIM1αβ KO mice (***B***). Statistical significance in ***A*** and ***B***: $*p < 0.05$, $**p < 0.005$. Representative traces at each ISI (superimposed after subtraction of the first response) are shown above. ***C***, ***D***, KO to wild-type ratios are shown for both mouse lines.

in these *in vitro* experiments, RIM1α KO neurons show a modest deficit in paired pulse responses, whereas they did not show such a deficit in slice analysis, might be due to the differences between the two experimental approaches. Cultured neurons and neurons in acute slices clearly have distinct properties. Furthermore, stimulus intensities are adjusted to evoke a response of a specific size in acute slices, whereas stimulus intensities in cultures are kept constant, and the response size is measured. Finally, in slices we specifically measured synaptic transmission in CA1 interneurons, whereas in mixed hippocampal cultures, CA3 interneurons predominate. It is important to note that the RIM1αβ KO phenotype after chronic deletion in the brains of the KO mice and after acute deletion *in vitro* is very similar. This observation rules out a major contribution of (1) compensatory mechanisms after chronic deletion of RIM1 isoforms in the constitutive KO and (2) mixed genetic backgrounds in the mice that were used for the slice analysis.

Presynaptic long-term plasticity is abolished in RIM1αβ KO mice

RIM1α is essential for several forms of presynaptic long-term plasticity that are mediated by an increase of cAMP and require presynaptic activation of protein kinase A (Hirano, 1991; Xiang et al., 1994; Nicoll and Schmitz, 2005). Such RIM1α dependent forms of long-term plasticity which are expressed as a presynaptic increase of neurotransmitter release are mf-LTP in excitatory mossy fiber synapses in the hippocampus, parallel fiber LTP at excitatory cerebellar granule-cell to Purkinje-cell synapses, and endocannabinoid-dependent I-LTD in the hippocampus and the amygdala (Castillo et al., 2002; Chevaleyre et al., 2007). Therefore, we tested whether presynaptic long-term plasticity is also affected in RIM1αβ KO mice (Fig. 9). We found that excitatory mf-LTP and inhibitory I-LTD were abolished in the hippocampus of RIM1αβ KO mice, demonstrating that RIM1αβ KO mice exhibit the same long-term plasticity phenotype as RIM1α KO mice.

Discussion

RIMs are scaffolding proteins of presynaptic active zones that perform a dual function in neurotransmitter release: they organize the basic release process (e.g., vesicle priming), and they are essential for presynaptic plasticity (e.g., mossy-fiber LTP). The most abundantly expressed *RIM* gene in forebrain is *RIM1* that was thought until now to produce only a single isoform, RIM1α. Previous studies uncovered essential roles for RIM1α in neurotransmitter release, but also demonstrated somewhat surprisingly that the protein was not required for survival (Castillo et al., 2002; Schoch et al., 2002). Here, we present four principal findings that change our view of the expression and role of the *RIM1* gene. We demonstrate (1) that the *RIM1* gene produces two independent RIM1 isoforms, RIM1α and a novel isoform called RIM1β, with the major difference between the two being that RIM1α contains, and RIM1β lacks, the N-terminal α-helix of α-RIMs that interacts with Rab3. We show (2) that deletion of both RIM1α and RIM1β impairs survival in mice, whereas deletion of RIM1α alone does not, probably because it causes compensatory upregulation of RIM1β that partly rescues the deletion of RIM1α. Among others, this finding demonstrates that at least some of the essential RIM functions do not require Rab3 binding. We find (3) that the amount and/or the solubility of all RIM-interacting active-zone proteins is altered in RIM1αβ KO mice, supporting the notion that RIM1α and RIM1β act as scaffolding proteins in the presynaptic active zone that physiologically bind to multiple other active zone proteins. We finally demonstrate (4) that the impairment in synaptic transmission observed in RIM1α KO mice is aggravated in RIM1αβ KO mice, whereas the block of long-term plasticity is the same. Thus, most RIM1-dependent functions, except for those in long-term synaptic plasticity, are executed independent of Rab3-binding by RIM1α.

RIM1β is a vital RIM isoform

Considering that RIM1β only accounts for ~10% of RIM1 isoforms, it is surprising that its deletion has such a drastic effect on mouse survival. The lethality of the RIM1αβ KO in contrast to the viability of the RIM1α KO mice is probably due to two factors. First, RIM1β is upregulated ~2-fold in the RIM1α KO mice (Fig. 1), and this helps to compensate for the loss of RIM1α by partly rescuing the KO phenotype. Second, RIM1β is prominently expressed in early postnatal development in the caudal brain regions such as the brainstem, which are critical for vital functions. In contrast, RIM1α is more abundant in rostral brain areas that are associated with cognitive functions. Our data, together with previous studies (Schoch et al., 2002, 2006), suggest a

dose-dependent effect of RIM deletions on survival. RIM1α or RIM2α KO mice survive almost normal, whereas the double deletion of RIM1α and RIM2α, or of RIM1α and RIM1β, severely reduces survival (Schoch et al., 2006) (Fig. 3).

Deletion of RIM1α and RIM1β has noteworthy effects on the composition of active zones (Fig. 4). The drastic reduction of Munc13-1 levels and the twofold increase in solubility of the remaining Munc13-1 in RIM1αβ KO mice agrees with the observation that the absence of RIM1α leads to decreased recruitment of Munc13-1 into the insoluble fraction (Andrews-Zwilling et al., 2006). We also found that three other active zone proteins displayed increased solubility in the RIM1αβ KO mice (ELKSs, RIM-BPs, α-liprins). These findings underline the central function of RIM1α and RIM1β as presynaptic scaffolding proteins that recruit and stabilize other components of the presynaptic active zone.

RIM1α and RIM1β both contribute to neurotransmitter release in the CA1 region of the hippocampus

Genetic studies of RIM function in synaptic transmission have focused on excitatory synapses, where deletion of RIM1α and RIM2α decreases release (Schoch et al., 2002, 2006; Calakos et al., 2004). Here, we also observed a major decrease in release at excitatory synapses in RIM1αβ KO mice, although the absence of a direct comparison of excitatory synaptic transmission in RIM1α and RIM1αβ KO mice makes it impossible to tell whether this decrease is more severe in RIM1αβ-deficient synapses than in RIM1α-deficient synapses.

Different from excitatory synapses, little was known about the role of RIMs in inhibitory synapses. Our data show that the deletion of RIM1α causes a reduction in input-output function and quantal release (as indicated by a reduction in mIPSC frequency but not amplitude) in inhibitory synapses in acute brain slices and a reduction of paired pulse depression in cultured neurons. Deletion of both RIM1α and RIM1β severely aggravated this inhibitory synapse phenotype (Figs. 6–8). Together, these results indicate that deletion of RIM1α decreases P_r at some inhibitory synapses, and that the additional deletion of RIM1β produces a further reduction in P_r. These results are apparently contradictory to our previous conclusion suggesting that, under certain recording conditions in acute brain slices, deletion of RIM1α induced an increase in P_r at inhibitory synapses (Schoch et al., 2002). Specifically, we previously found that RIM1α KO mice show increased paired-pulse depression of IPSCs at a short ISI of 20 ms. Consistent with these previous observations, we confirm here that paired-pulse depression in RIM1α KO mice is indistinguishable from wild-type mice under recording conditions of relatively high initial P_r (e.g., 2.5 mM Ca^{2+}, 1.3 mM Mg^{2+}). Overall however, these results suggest that the role of RIM1α in basic neu-

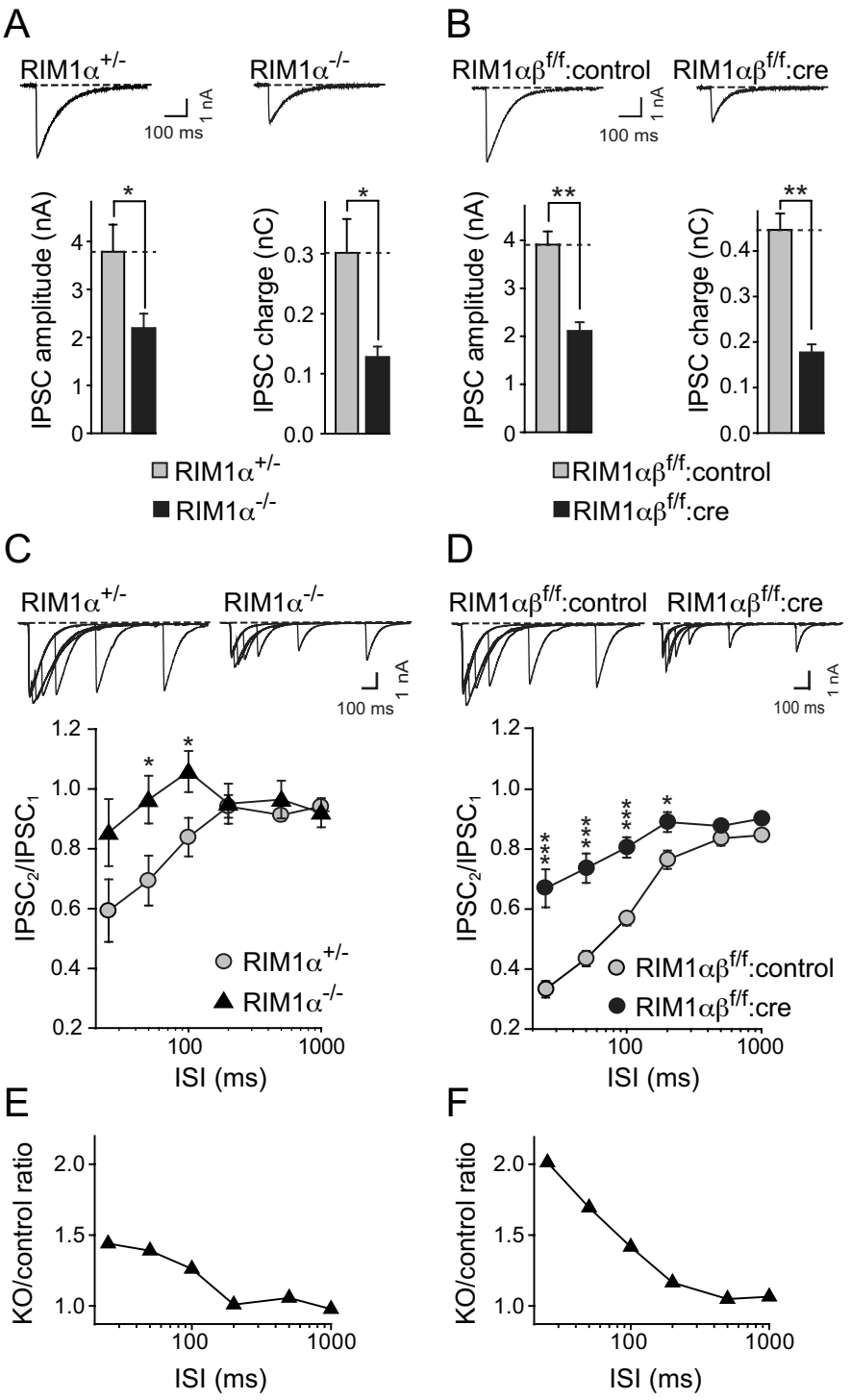

Figure 8. Synaptic transmission in cultured hippocampal neurons lacking RIM1α or RIM1α and RIM1β deficient neurons. ***A***, Evoked single inhibitory responses in cultured neurons at DIV 13–16 derived from newborn RIM1α KO mice and heterozygous control mice, IPSC charge and amplitude were quantified. ***B***, The same experiment was performed in cultured neurons from newborn RIM1$\alpha\beta^{floxed}$ mice, and cultures were infected with lentivirus expressing cre recombinase (RIM1$\alpha\beta^{f/f}$:cre) or a recombination deficient deletion mutant of cre (RIM1$\alpha\beta^{f/f}$:control). ***C***, ***D***, Paired pulse experiments in cultures that lack RIM1α (***C***) or RIM1αβ (***D***) and corresponding control cultures. Sample traces are given on top. ***E***, ***F***, KO to control ratios of the paired pulse experiments for both lines. Statistical significance in ***A–D***: $*p < 0.05$, $**p < 0.005$, $***p < 0.0005$.

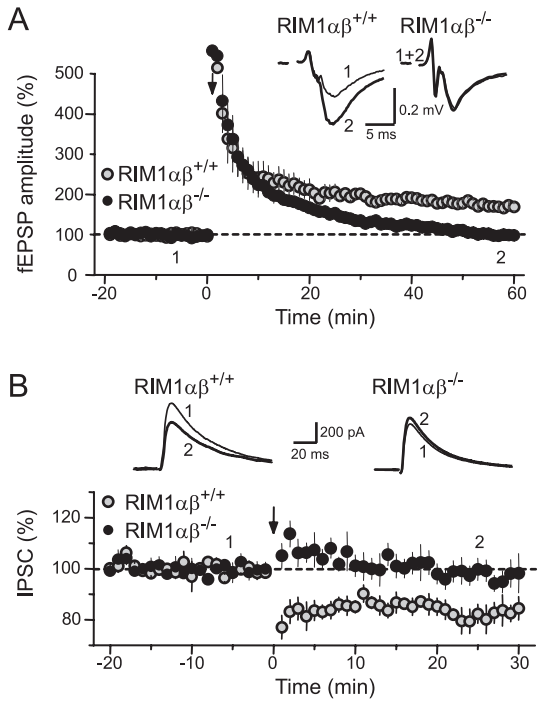

Figure 9. Presynaptic forms of long-term plasticity in the hippocampus of RIM1αβ KO mice. ***A***, Time course of mossy fiber fEPSP amplitude in CA3. LTP was triggered by a burst of 125 stimuli at 25 Hz (arrow). Top inset, Sample traces from representative experiments obtained at the time points indicated. Each trace is the average of 5 min of recording. Statistical significance before versus after induction: RIM1αβ wild-type, $p < 0.00001$; RIM1αβ KO, $p > 0.05$. ***B***, Time course of IPSC amplitude in whole-cell recordings in CA1. I-LTD was triggered by theta-burst stimulation (arrow). Top, Sample traces from representative experiments obtained at the time points indicated. Each trace is the average of 10 min of recording. Statistical significance before versus after induction: RIM1αβ wild-type, $p < 0.001$; RIM1αβ KO, $p > 0.5$.

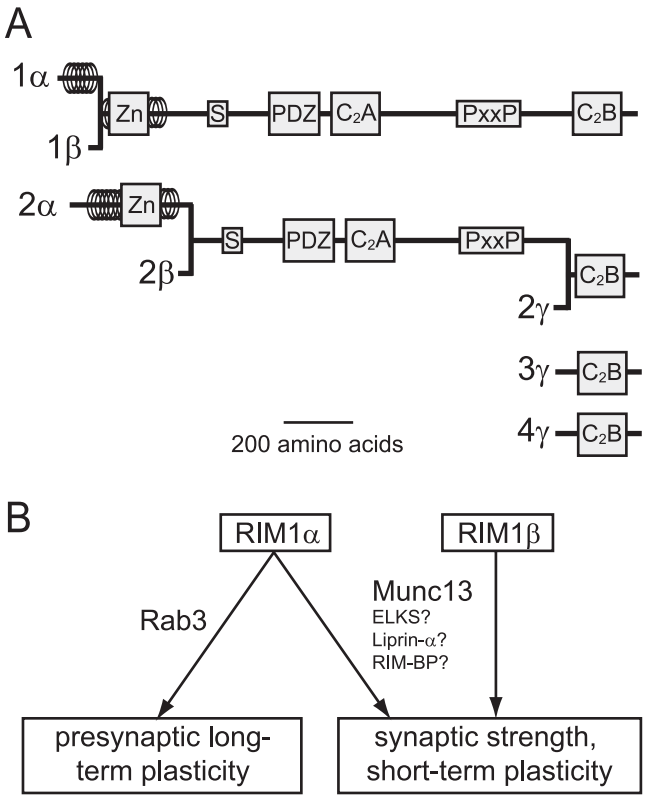

Figure 10. RIM isoforms and RIM1-centered functional model of regulation of presynaptic neurotransmitter release. ***A***, Overview of RIM isoforms of the 4 mammalian *RIM* genes. ***B***, RIM1α and RIM1β regulate presynaptic plasticity distinctively. RIM1α and RIM1β mediate short-term plasticity and synaptic strength through Munc13 and other proteins. In addition, RIM1α is required for normal long-term plasticity through its interaction with Rab3. RIM1β does not participate in long-term plasticity, consistent with the absence of the Rab3 binding α-helix. Our data support a mechanism where these parameters are regulated through distinct coupling of RIM1α and RIM1β to Rab3 and/or Munc13.

rotransmitter release processes may be very similar at inhibitory and excitatory synapses, and resemble that of RIM1β.

RIM1β acts independently of Rab3

RIM1β lacks the N-terminal α-1 helix of RIM1α that is necessary and sufficient for Rab3 binding (Wang et al., 2001; Fukuda, 2004; Dulubova et al., 2005), but contains the zinc-finger domain that binds to Munc13 s (Fig. 10*A*). Thus, the phenotypic difference between RIM1α and RIM1αβ KO mice uncovers mechanistic differences between Rab3-dependent and Rab3-independent activities of RIM1. In this regard, our results suggest that most RIM functions are Rab3-independent since the presence of RIM1β partially rescues most of the RIM1α KO phenotype, but that one particular activity of RIM1, namely its role in long-term synaptic plasticity, is mediated by Rab3 binding because the RIM1α KO phenotype in long-term plasticity is not further aggravated by the RIM1αβ KO, nor is it rescued by upregulated expression of RIM1β in the RIM1α KO mice.

It is important to note here that our findings support the crucial importance of the interplay between RIM1α and Rab3 in multiple forms of long-term presynaptic plasticity (Castillo et al., 1997, 2002; Huang et al., 2005; Chevaleyre et al., 2007). Indeed, the present findings suggest an explanation for our previous observation of a surprising phenotypic dichotomy in RIM1α KO mice. This dichotomy was observed in synapses that express presynaptic long-term plasticity, and in which deletion of RIM1α abolished such plasticity, but did not cause the same impairment in basic release properties and short-term plasticity that was observed in other synapses (Castillo et al., 2002; Schoch et al., 2002). Our present findings now show that this impairment in basic release properties is observed in synapses capable of presynaptic long-term plasticity in RIM1αβ KO mice, in addition to the blocked long-term presynaptic plasticity. Thus, the increased RIM1β levels in the RIM1α KO mice appear to rescue the changes in basic release properties in these synapses, but cannot rescue the lack of long-term plasticity since RIM1β does not bind Rab3. The question arises why the increased RIM1β levels in RIM1α KO mice cannot rescue all of this basic release phenotype in all synapses, but only in synapses competent for long-term presynaptic plasticity. Although a definitive answer to this question is not possible at present, it is possible that the levels of different RIM isoforms (Fig. 10*A*) may differ among the various types of synapses, thereby accounting for this discrepancy.

Differential functions of RIM1 isoforms in neurotransmission

Based on our analysis of the RIM1αβ KO mice, we would like to propose a model of the role of RIM1α and RIM1β in synaptic transmission (Fig. 10*B*). This model suggests that RIM1α and RIM1β redundantly mediate most basic processes in synaptic vesicle exocytosis via interactions with Munc13-1 and other synaptic proteins that are performed by both isoforms. In contrast, the function of RIM1α in long-term synaptic plasticity requires its binding to Rab3, possibly by coupling Rab3-binding to the interactions of RIM with other active zone proteins. This special

Rab3-dependent function of RIM1α is the same in RIM1α and RIM1αβ KO mice because RIM1β does not normally contribute to it. More recent observations have suggested that cellular mechanism other than the interactions outlined in Figure 10*B* such as phosphorylation and ubiquitination might be involved in regulating RIM1 dependent neurotransmitter release (Inoue et al., 2006; Yao et al., 2007), but it remains to be elucidated which RIM1 isoforms may be a target of these modifications and how this could affect neurotransmitter release *in vivo*. Overall, our data underline the importance of dissecting the function of active zone proteins by targeting discrete isoforms of participating proteins. It will be fascinating to find specific contributions of other β-RIMs and γ-RIMs (Fig. 10*A*), and to finally assign concrete roles to each biochemical interaction of RIMs at the presynaptic active zone. Generating a conditional KO mouse for RIM1αβ as reported here represents a first step to achieve this long-term goal.

References

Andrews-Zwilling YS, Kawabe H, Reim K, Varoqueaux F, Brose N (2006) Binding to Rab3A-interacting molecule RIM regulates the presynaptic recruitment of Munc13-1 and ubMunc13–2. J Biol Chem 281:19720–19731.

Betz A, Thakur P, Junge HJ, Ashery U, Rhee JS, Scheuss V, Rosenmund C, Rettig J, Brose N (2001) Functional interaction of the active zone proteins Munc13-1 and RIM1 in synaptic vesicle priming. Neuron 30:183–196.

Calakos N, Schoch S, Südhof TC, Malenka RC (2004) Multiple roles for the active zone protein RIM1alpha in late stages of neurotransmitter release. Neuron 42:889–896.

Castillo PE, Janz R, Südhof TC, Tzounopoulos T, Malenka RC, Nicoll RA (1997) Rab3A is essential for mossy fibre long-term potentiation in the hippocampus. Nature 388:590–593.

Castillo PE, Schoch S, Schmitz F, Südhof TC, Malenka RC (2002) RIM1alpha is required for presynaptic long-term potentiation. Nature 415:327–330.

Chevaleyre V, Heifets BD, Kaeser PS, Südhof TC, Purpura DP, Castillo PE (2007) Endocannabinoid-mediated long-term plasticity requires cAMP/PKA signaling and RIM1alpha. Neuron 54:801–812.

Coppola T, Magnin-Luthi S, Perret-Menoud V, Gattesco S, Schiavo G, Regazzi R (2001) Direct interaction of the Rab3 effector RIM with Ca2+ channels, SNAP-25, and synaptotagmin. J Biol Chem 276:32756–32762.

Dai H, Tomchick DR, García J, Südhof TC, Machius M, Rizo J (2005) Crystal structure of the RIM2 C2A-domain at 1.4 A resolution. Biochemistry 44:13533–13542.

Dulubova I, Lou X, Lu J, Huryeva I, Alam A, Schneggenburger R, Südhof TC, Rizo J (2005) A Munc13/RIM/Rab3 tripartite complex: from priming to plasticity? EMBO J 24:2839–2850.

Dymecki SM (1996) Flp recombinase promotes site-specific DNA recombination in embryonic stem cells and transgenic mice. Proc Natl Acad Sci U S A 93:6191–6196.

Fukuda M (2004) Alternative splicing in the first alpha-helical region of the Rab-binding domain of Rim regulates Rab3A binding activity: is Rim a Rab3 effector protein during evolution? Genes Cells 9:831–842.

Hessler NA, Shirke AM, Malinow R (1993) The probability of transmitter release at a mammalian central synapse. Nature 366:569–572.

Hibino H, Pironkova R, Onwumere O, Vologodskaia M, Hudspeth AJ, Lesage F (2002) RIM binding proteins (RBPs) couple Rab3-interacting molecules (RIMs) to voltage-gated Ca(2+) channels. Neuron 34:411–423.

Hirano T (1991) Differential pre- and postsynaptic mechanisms for synaptic potentiation and depression between a granule cell and a Purkinje cell in rat cerebellar culture. Synapse 7:321–323.

Ho A, Morishita W, Atasoy D, Liu X, Tabuchi K, Hammer RE, Malenka RC, Südhof TC (2006) Genetic analysis of Mint/X11 proteins: essential presynaptic functions of a neuronal adaptor protein family. J Neurosci 26:13089–13101.

Huang YY, Zakharenko SS, Schoch S, Kaeser PS, Janz R, Südhof TC, Siegelbaum SA, Kandel ER (2005) Genetic evidence for a protein-kinase-A-mediated presynaptic component in NMDA-receptor-dependent forms of long-term synaptic potentiation. Proc Natl Acad Sci U S A 102:9365–9370.

Inoue E, Mochida S, Takagi H, Higa S, Deguchi-Tawarada M, Takao-Rikitsu E, Inoue M, Yao I, Takeuchi K, Kitajima I, Setou M, Ohtsuka T, Takai Y (2006) SAD: a presynaptic kinase associated with synaptic vesicles and the active zone cytomatrix that regulates neurotransmitter release. Neuron 50:261–275.

Kaeser PS, Südhof TC (2005) RIM function in short- and long-term synaptic plasticity. Biochem Soc Trans 33:1345–1349.

Kaeser PS, Kwon HB, Blundell J, Chevaleyre V, Morishita W, Malenka RC, Powell CM, Castillo PE, Südhof TC (2008) RIM1alpha phosphorylation at serine-413 by protein kinase A is not required for presynaptic long-term plasticity or learning. Proc Natl Acad Sci U S A 105:14680–14685.

Katz B, Miledi R (1967) The timing of calcium action during neuromuscular transmission. J Physiol 189:535–544.

Kiyonaka S, Wakamori M, Miki T, Uriu Y, Nonaka M, Bito H, Beedle AM, Mori E, Hara Y, De Waard M, Kanagawa M, Itakura M, Takahashi M, Campbell KP, Mori Y (2007) RIM1 confers sustained activity and neurotransmitter vesicle anchoring to presynaptic Ca2+ channels. Nat Neurosci 10:691–701.

Koushika SP, Richmond JE, Hadwiger G, Weimer RM, Jorgensen EM, Nonet ML (2001) A post-docking role for active zone protein Rim. Nat Neurosci 4:997–1005.

Maximov A, Pang ZP, Tervo DG, Südhof TC (2007) Monitoring synaptic transmission in primary neuronal cultures using local extracellular stimulation. J Neurosci Methods 161:75–87.

Maximov A, Lao Y, Li H, Chen X, Rizo J, Sørensen JB, Südhof TC (2008) Genetic analysis of synaptotagmin-7 function in synaptic vesicle exocytosis. Proc Natl Acad Sci U S A 105:3986–3991.

Monier S, Jollivet F, Janoueix-Lerosey I, Johannes L, Goud B (2002) Characterization of novel Rab6-interacting proteins involved in endosome-to-TGN transport. Traffic 3:289–297.

Nakata T, Kitamura Y, Shimizu K, Tanaka S, Fujimori M, Yokoyama S, Ito K, Emi M (1999) Fusion of a novel gene, ELKS, to RET due to translocation t(10;12)(q11;p13) in a papillary thyroid carcinoma. Genes Chromosomes Cancer 25:97–103.

Nicoll RA, Schmitz D (2005) Synaptic plasticity at hippocampal mossy fibre synapses. Nat Rev Neurosci 6:863–876.

O'Gorman S, Dagenais NA, Qian M, Marchuk Y (1997) Protamine-Cre recombinase transgenes efficiently recombine target sequences in the male germ line of mice, but not in embryonic stem cells. Proc Natl Acad Sci U S A 94:14602–14607.

Ohtsuka T, Takao-Rikitsu E, Inoue E, Inoue M, Takeuchi M, Matsubara K, Deguchi-Tawarada M, Satoh K, Morimoto K, Nakanishi H, Takai Y (2002) Cast: a novel protein of the cytomatrix at the active zone of synapses that forms a ternary complex with RIM1 and Munc13-1. J Cell Biol 158:577–590.

Ozaki N, Shibasaki T, Kashima Y, Miki T, Takahashi K, Ueno H, Sunaga Y, Yano H, Matsuura Y, Iwanaga T, Takai Y, Seino S (2000) cAMP-GEFII is a direct target of cAMP in regulated exocytosis. Nat Cell Biol 2:805–811.

Rosahl TW, Geppert M, Spillane D, Herz J, Hammer RE, Malenka RC, Südhof TC (1993) Short-term synaptic plasticity is altered in mice lacking synapsin I. Cell 75:661–670.

Rosenmund C, Clements JD, Westbrook GL (1993) Nonuniform probability of glutamate release at a hippocampal synapse. Science 262:754–757.

Schoch S, Gundelfinger ED (2006) Molecular organization of the presynaptic active zone. Cell Tissue Res 326:379–391.

Schoch S, Castillo PE, Jo T, Mukherjee K, Geppert M, Wang Y, Schmitz F, Malenka RC, Südhof TC (2002) RIM1alpha forms a protein scaffold for regulating neurotransmitter release at the active zone. Nature 415:321–326.

Schoch S, Mittelstaedt T, Kaeser PS, Padgett D, Feldmann N, Chevaleyre V, Castillo PE, Hammer RE, Han W, Schmitz F, Lin W, Südhof TC (2006) Redundant functions of RIM1alpha and RIM2alpha in Ca(2+)-triggered neurotransmitter release. EMBO J 25:5852–5863.

Simsek-Duran F, Linden DJ, Lonart G (2004) Adapter protein 14–3-3 is required for a presynaptic form of LTP in the cerebellum. Nat Neurosci 7:1296–1298.

Steeg CM, Ellis J, Bernstein A (1990) Introduction of specific point mutations into RNA polymerase II by gene targeting in mouse embryonic stem cells: evidence for a DNA mismatch repair mechanism. Proc Natl Acad Sci U S A 87:4680–4684.

Sudhof TC (2004) The synaptic vesicle cycle. Annu Rev Neurosci 27:509–547.

Sun L, Bittner MA, Holz RW (2003) RIM, a component of the presynaptic active zone and modulator of exocytosis, binds 14–3-3 through its N-terminus. J Biol Chem 278:38301–38309.

Wang X, Hu B, Zimmermann B, Kilimann MW (2001) Rim1 and rabphilin-3 bind Rab3-GTP by composite determinants partially related through N-terminal alpha -helix motifs. J Biol Chem 276:32480–32488.

Wang Y, Südhof TC (2003) Genomic definition of RIM proteins: evolutionary amplification of a family of synaptic regulatory proteins(small star, filled). Genomics 81:126–137.

Wang Y, Okamoto M, Schmitz F, Hofmann K, Sudhof TC (1997) Rim is a putative Rab3 effector in regulating synaptic-vesicle fusion. Nature 388:593–598.

Wang Y, Sugita S, Sudhof TC (2000) The RIM/NIM family of neuronal C2 domain proteins. Interactions with Rab3 and a new class of Src homology 3 domain proteins. J Biol Chem 275:20033–20044.

Wang Y, Liu X, Biederer T, Südhof TC (2002) A family of RIM-binding proteins regulated by alternative splicing: Implications for the genesis of synaptic active zones. Proc Natl Acad Sci U S A 99:14464–14469.

Xiang Z, Greenwood AC, Kairiss EW, Brown TH (1994) Quantal mechanism of long-term potentiation in hippocampal mossy-fiber synapses. J Neurophysiol 71:2552–2556.

Yao I, Takagi H, Ageta H, Kahyo T, Sato S, Hatanaka K, Fukuda Y, Chiba T, Morone N, Yuasa S, Inokuchi K, Ohtsuka T, Macgregor GR, Tanaka K, Setou M (2007) SCRAPPER-dependent ubiquitination of active zone protein RIM1 regulates synaptic vesicle release. Cell 130:943–957.